Supporting Information

for

Legitimate Intermediates of Oxygen Evolution on Iridium Oxide Revealed by *In-situ* Electrochemical Evanescent Wave Spectroscopy

Hideshi Ooka,[†] Yuanqing Wang,[‡] Akira Yamaguchi,[‡] Makoto Hatakeyama,[#] Shinichiro Nakamura,[#] Kazuhito Hashimoto,[†*] and Ryuhei Nakamura[‡]

† Department of Applied Chemistry, The University of Tokyo, 7-3-1 Hongo, Bunkyo-ku, Tokyo 113-8656, Japan

‡ Biofunctional Catalyst Research Team, RIKEN Center for Sustainable Resource Science, 2-1 Hirosawa, Wako, Saitama 351-0198, Japan

Computational Chemistry Applications Unit, Advanced Center for Computing and Communication, 2-1 Hirosawa, Wako, Saitama 351-0198, Japan

Table of Contents

Additional Notes on the Computational Procedure

DFT calculations were performed to search the possible intermediates revealed by *in-situ* EW spectroscopy. Detailed justification of the binuclear model (see Fig. S7) will be given in alternative reference.[1] Briefly, the binuclear model is based on the previously justified manganese dimer for the oxygen evolution reaction.[2] As shown in table S1, the quintet state is found to have the lowest energy within the optimized structure of each spin state of the Ir^{V} binuclear cluster. The results obtained with and without symmetry constraint, and in gas phase and in aqueous phase (PCM solvation model), show the same trend in terms of energy difference. The energy calculated from the antiferromagnetic singlet state presents no noticeable difference from that at quintet state. In addition to the comparison performed between the optimized structures, electronic energy calculation in fixed geometry is also performed as shown in table S2 and S3. It is found that in the case of O-O bond formed structures, the triplet state has the lowest energy; while in the case without O-O bond formation, the quintet state is the lowest. Therefore, these two species were studied further with potential energy surface scan in PCM model. As shown in Fig. 4B, the potential energy curve of the Ir^{v} binuclear cluster in the quintet state shows that the electronic energy increases upon increase in O-O distance, indicating that O-O bond formation is unfavorable. In contrast, considering both the potential energy curve of the Ir^{v} binuclear cluster in the quintet and triplet states, the results indicate the presence of a species in the triplet state which can lead to O-O bond formation later. (see Fig. 4B). Thus, the corresponding structure was searched and found (with zero imaginary frequencies) in triplet state prior to O-O bond formation (Fig. S7, Table S5).

Based on the above discussion, the absorption spectrum of the lowest energy Ir^{v} binuclear cluster in quintet state is simulated. As shown in Fig. 4A, the simulated peak is found at ~399 nm comparable to the experimentally observed peak at ~410 nm, which suggests that the Ir^{v} species found in experiment possesses an Ir-O moiety. The experimental results indicate that the species leading to the red shift is ascribed to structure prior to O-O bond formation. From Fig. 4A, the simulated spectrum of the structure in the triplet state presents two peaks at ~396 nm and ~491 nm and the differential spectrum is comparable to the experimental red shift at ~490 nm (Fig. 3C). Compared with the structure in quintet state, one Ir-O bond length extended from ~178 pm to 189 pm. These results suggest that the observed red shift is due to the structural change along with the spin state change from the quintet state to the triplet state leading to O-O bond formation.

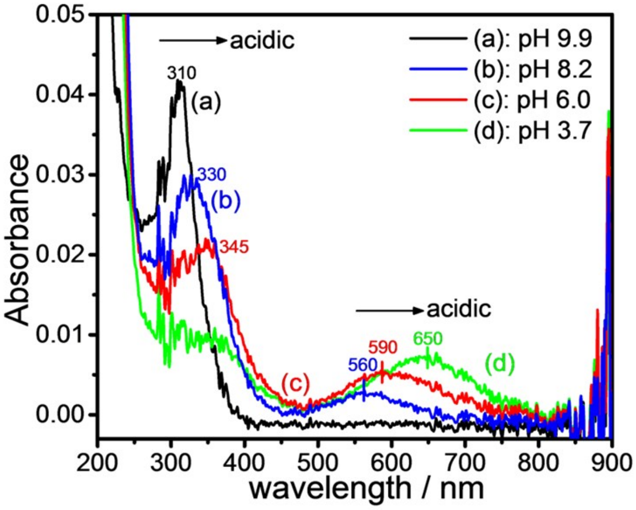

Fig. S1. Diffuse transmission UV-Vis spectrum of the deposition solution at pH 3.7-9.9. pH adjustments were performed by addition of HCl and NaOH.

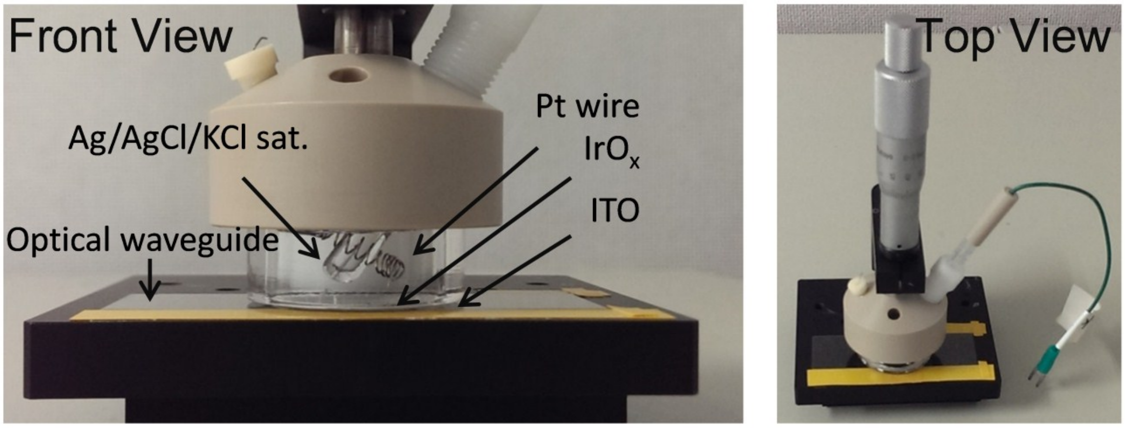

Fig. S2. Experimental setup of the optical waveguide and the custom made electrochemical chamber from the front (left panel) and the top (right panel).

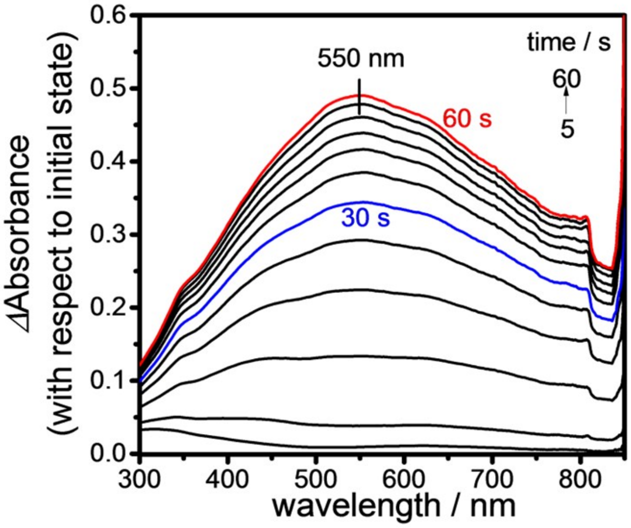

Fig. S3. UV-Vis EW spectra of the ITO electrode during electrodeposition at constant current (25 μAcm^{-2}). Spectra were recorded every 5 seconds by taking the spectrum before electrodeposition as the reference. Blue and red spectra are the spectra taken at 30 and 60 seconds after electrodeposition was initiated. The broad absorption at 550 nm indicate the formation of Ir^{IV} oxides.

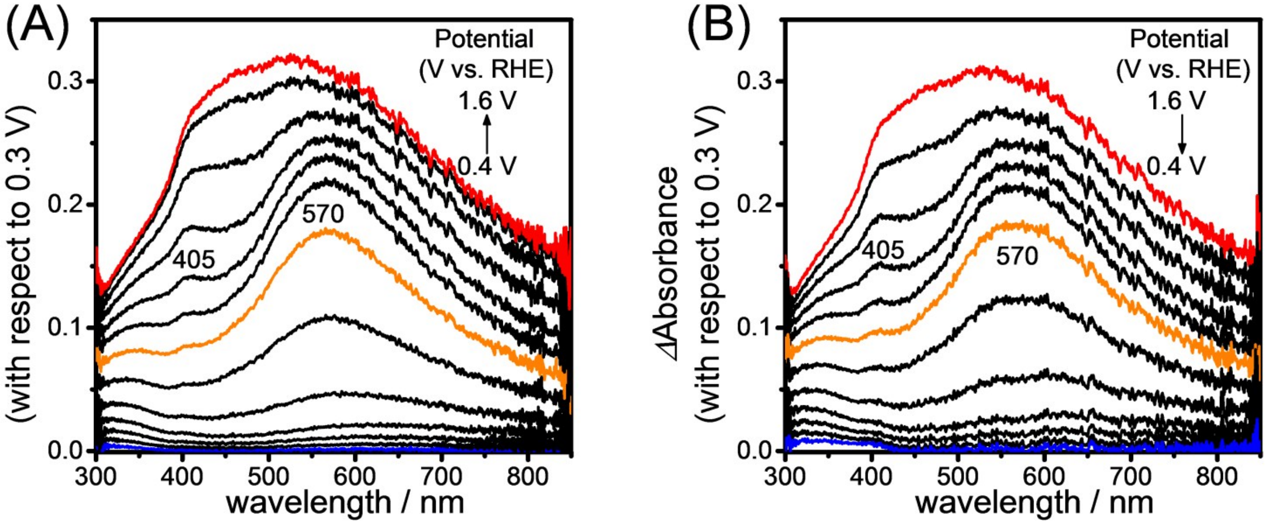

Fig. S4. UV-Vis EW spectra of the iridium oxide electrode in 0.5 M Na_2SO_4 (pH 2) by taking the spectrum at 0.3 V vs RHE as the reference. Blue, orange, and red lines correspond to the spectrum at 0.4 V, 1.0 V, and 1.6 V respectively. Anodic scan (A) and cathodic scan (B).

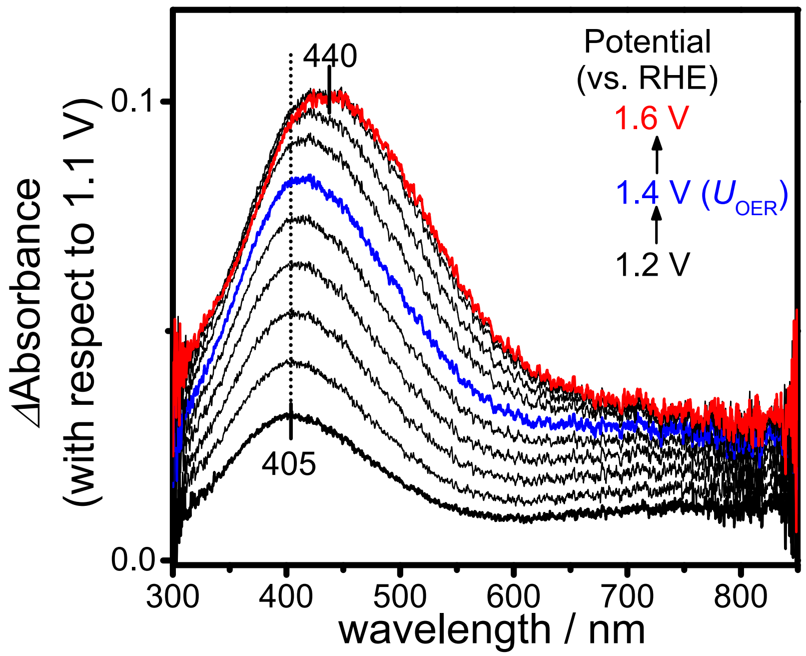

Fig. S5. UV-Vis EW spectra of the iridium oxide electrode in 0.5 M Na_2SO_4 (pH 12) by taking the spectrum at 1.1 V vs RHE as the reference. Blue and red lines correspond to the spectrum at 1.4 V (onset potential of oxygen evolution, U_{OER}) and 1.6 V respectively.

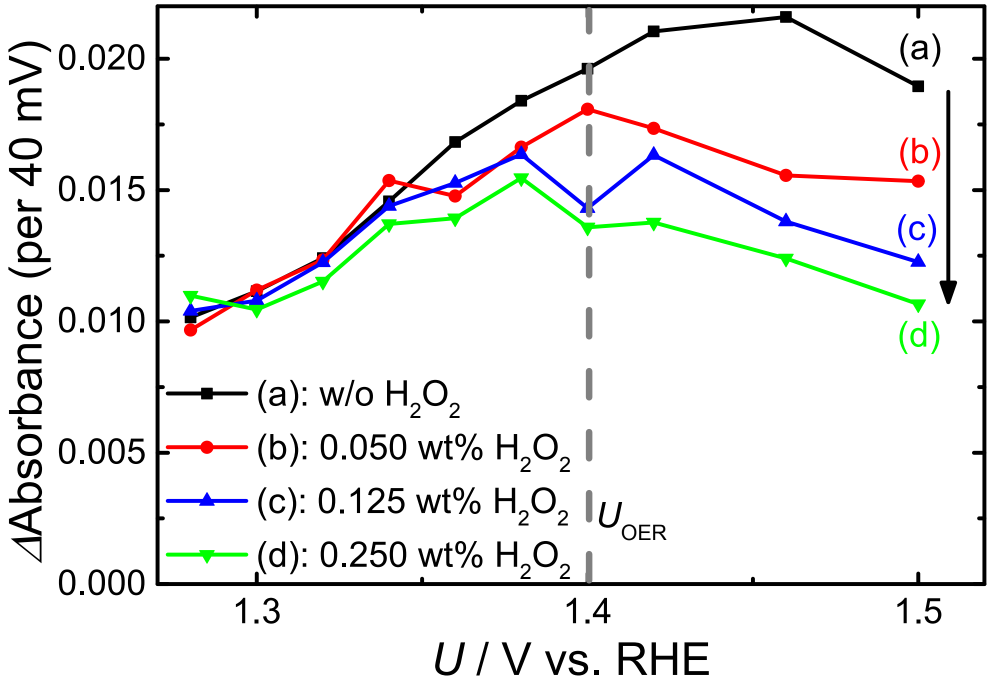

Fig. S6. Potential dependence of the absorption increase corresponding to species A_{450} generation under various concentrations of H_2O_2. (a): without H2O2, (b): 0.050 wt%, (c): 0.125 wt%, (d): 0.250 wt%

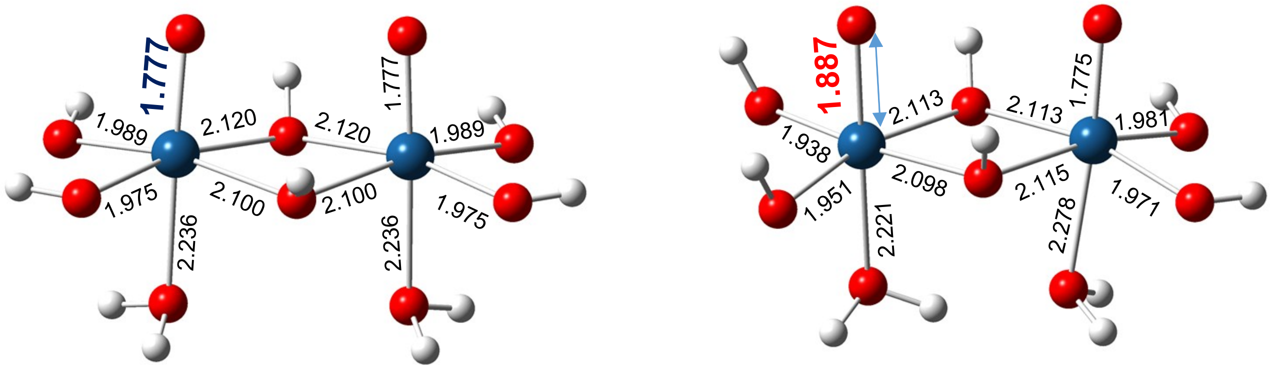

quintet triplet

Fig. S7. Geometry and bond lengths of the binuclear iridium oxide cluster within PCM model.

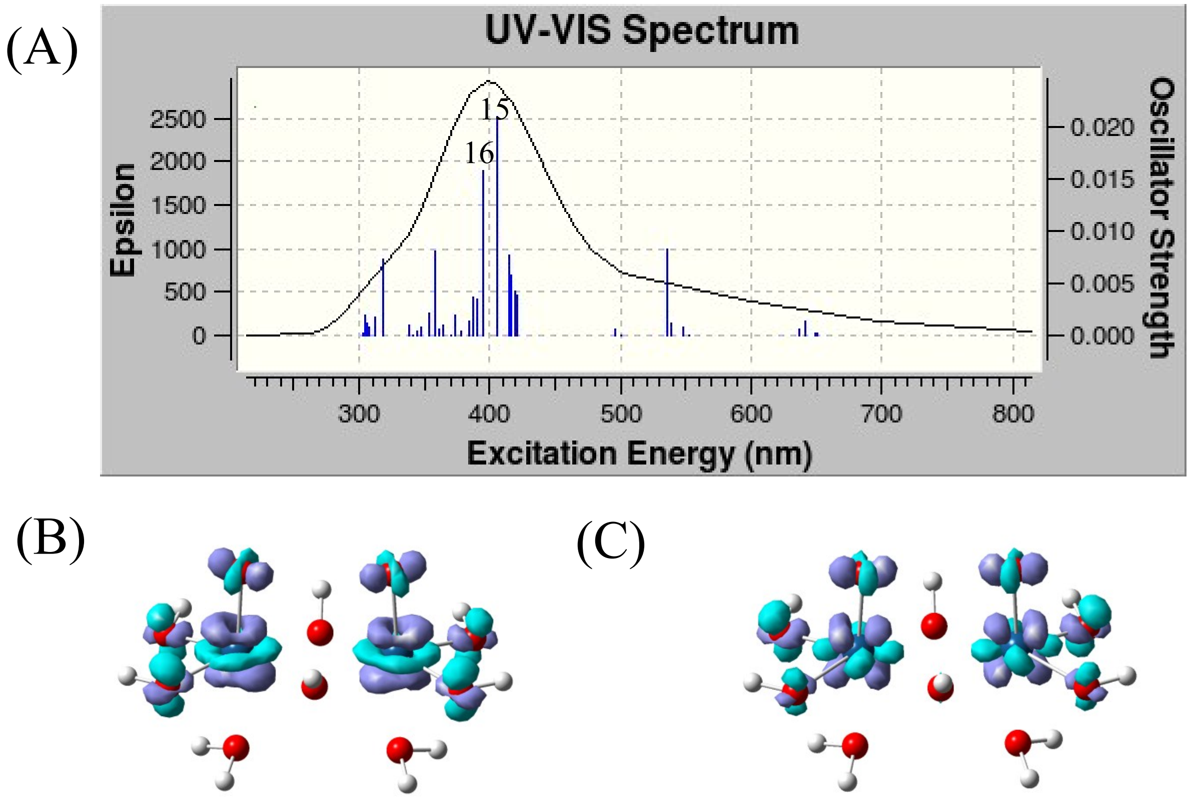

Fig. S8. Simulated UV-Vis absorption spectrum of a binuclear iridium oxide cluster in the quintet state (A). Differential electron density upon excitation to excited state 15 (B) and 16 (C). Turquoise and blue colors show regions (isovalue=0.006) of decreasing and increasing electron density, respectively.

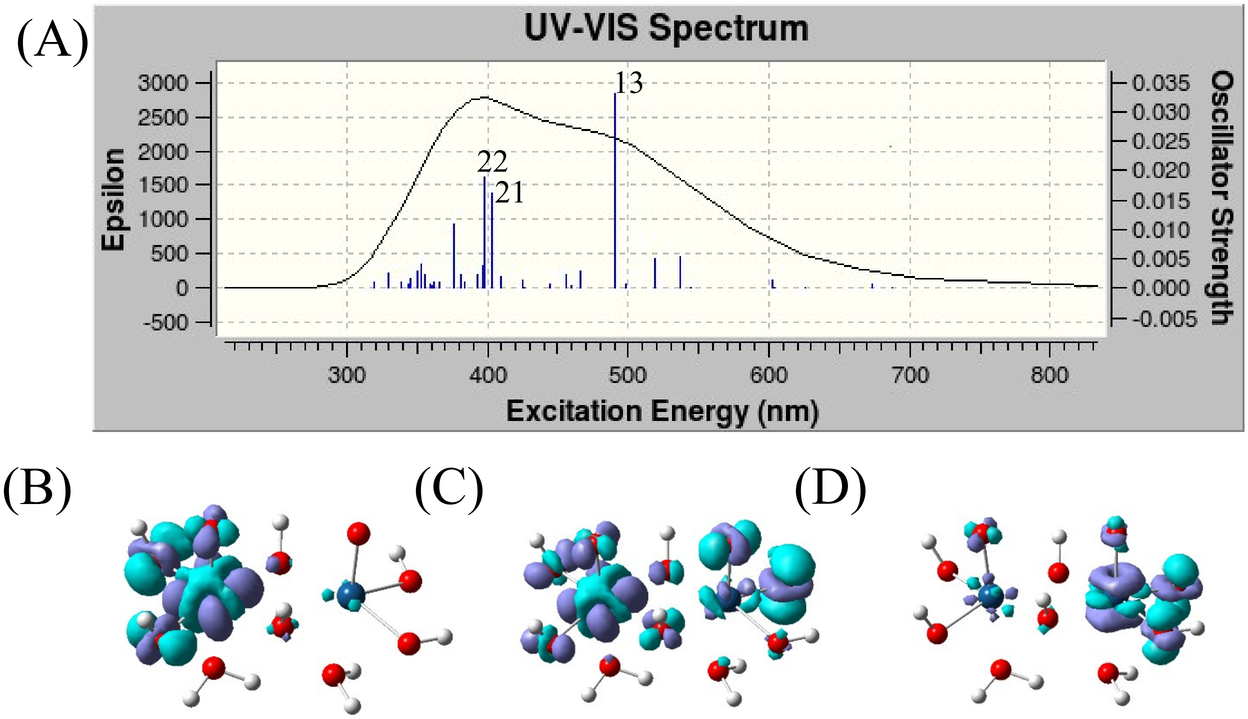

Fig. S9. Simulated UV-Vis absorption spectrum of a binuclear iridium oxide cluster in the triplet state (A). Differential electron density upon excitation to excited state 13 (B), 21 (C) and 22 (D). Turquoise and blue colors show regions (isovalue=0.006) of decreasing and increasing electron density, respectively.

Table S1 Relative energies of optimized Ir^{V} binuclear cluster in different spin states in gas phase (kcal/mol)

* For cases with energies much larger (>30 kcal/mol) than that in the quintet state, the corresponding calculations without symmetry constraint are not further studied.

Spin state	*Energy C_{2v} symmetry in gas phase*	*Energy without symmetry constraint in gas phase*	*Energy without symmetry constraint in aqueous solution (PCM)*
singlet	13.03	10.89	13.23
triplet	8.43	3.02	4.58
quintet	0.00	0.00	0.00
septet	57.34	-*	-*
nonet	82.41	-*	-*
antiferromagnetic singlet	-	0.03	0.14

Table S2 Relative energies of Ir^{V} binuclear cluster at different states in fixed geometry (obtained in quintet state without symmetry constraint in Table S1) in gas phase (kcal/mol)

Spin state	*Energy*
singlet	61.14
triplet	7.15
quintet	0.00
septet	68.16
nonet	138.25

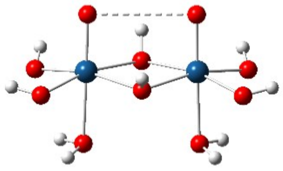

Calculated structure

Table S3 Relative energies of Ir^{V} binuclear cluster at different states in fixed geometry (obtained in triplet state without symmetry constraint in Table S1) in gas phase (kcal/mol)

Spin state	*Energy*
singlet	19.19
triplet	0.00
quintet	58.25
septet	123.45
nonet	178.47

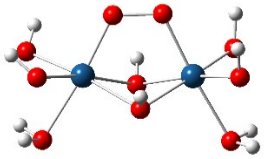

Calculated structure

Table S4 Molecular coordinates of the Ir^{V} binuclear cluster in the quintet state.

Atom		*Coordinates*	
Ir	-1.65167000	-0.10316400	0.19558000
Ir	1.65088500	-0.10145700	0.19857400
H	-2.89929400	2.05968600	0.22599400
H	-0.00191800	1.90914800	0.74450700
H	2.89624100	2.06267900	0.23023200
H	3.88892400	-1.03864700	-0.02744300
H	0.00050900	-2.19267800	0.43922300
H	-3.88839300	-1.04234000	-0.03467400
O	-3.17600400	1.16050300	0.00973400
O	-3.03193100	-1.49356500	-0.05013300
O	-0.00097500	1.22045300	0.06782500
O	0.00053400	-1.37187300	-0.06919400
O	3.17426400	1.16366800	0.01494100
O	3.03288100	-1.49060700	-0.04439100
H	2.45461500	0.59651600	-2.23616200
H	1.89501200	-0.83781600	-2.42128100
H	-1.89205100	-0.83930100	-2.42448100
H	-2.45085200	0.59543600	-2.24056500
O	1.55926600	-0.15344600	1.97292400
O	-1.56310500	-0.15543400	1.97006900
O	1.69575700	0.02689500	-2.03308400
O	-1.69269100	0.02534300	-2.03618800

Table S5 Molecular coordinates of the Ir^{V} binuclear cluster in the triplet state.

Atom		*Coordinates*	
Ir	-1.58006000	0.06317600	0.19203500
Ir	1.69617900	-0.14419100	0.05454500
H	-3.73154300	1.12656700	-0.23350900
H	0.23474300	1.80542900	0.92273000
H	3.46726800	1.55153100	0.43060800
H	3.36135200	-1.69161900	0.88018300
H	-0.03718600	-1.97357300	0.88566800
H	-2.88167100	-2.04135600	-0.00822100
O	-2.85067200	1.52453500	-0.17367300
O	-3.12420700	-1.12206000	-0.17796900
O	0.15257200	1.27458300	0.11762300
O	-0.02526700	-1.36647600	0.13417700
O	3.05325700	1.19269100	-0.36525500
O	2.88348300	-1.67606400	0.03573500
H	0.55900100	-0.10864700	-2.41800300
H	2.04135100	0.36136500	-2.59298900
H	-1.88609500	-0.64632800	-2.43335700
H	-1.72820400	0.89669200	-2.38960500
O	1.87458800	-0.02672100	1.92917000
O	-1.62453400	0.06908900	1.96613100
O	1.47952900	-0.29115400	-2.15065300
O	-1.33420700	0.06697900	-2.07260900

References

(1) Wang, Y.; Ooka, H.; Nakamura, S.; Nakamura, R. *In preparation*.

(2) Busch, M.; Ahlberg, E.; Panas, I. *PhysChemChemPhys* **2011,** *13*, 15069-15076.